ACS Energy LETTERS

http://pubs.acs.org/journal/aelccp

# Electrochemical $CO_2$ Reduction to Formic Acid with High Carbon Efficiency

Ahmad Elgazzar, Peng Zhu, Feng-Yang Chen, Shaoyun Hao, Tae-Ung Wi, Chang Qiu, Valery Okatenko, and Haotian Wang*

Cite This: *ACS Energy Lett.* 2025, 10, 450−458

Read Online

ACCESS | Metrics & More | Article Recommendations | Supporting Information

**ABSTRACT:** While much of the current research in electrochemical $CO_2$ reduction reaction ($CO_2RR$) identified the $CO_2$ single-pass conversion efficiency (SPCE) as a key performance metric for the technology practical deployment, recently reported high SPCEs in $CO_2RR$ are typically at the expense of higher cell voltages or compromised product selectivity. In this work, we use the porous solid electrolyte (PSE) reactor to achieve high $CO_2$ SPCE to high-purity formic acid (HCOOH) while preserving the cell voltage and HCOOH Faradaic efficiency. We successfully recovered the carbon losses in the PSE system to reach a 95.1 ± 1.7% $CO_2$ SPCE to HCOOH at 100 mA $cm^{-2}$ and demonstrated a stable operation for 100 h. To widen the applicability of the $CO_2RR$ technology, we demonstrate a continuous simulated flue gas (10% $CO_2$, 10% $O_2$, balance $N_2$) conversion to high-purity formic acid with $CO_2$ SPCE reaching more than 80% through an electrochemical sequential $CO_2$ capture−$CO_2$ reduction system.

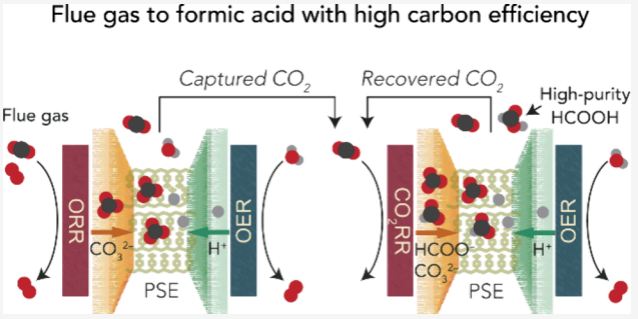


Ranked as the largest consumer of industrial energy and the third-largest subsector in direct $CO_2$ emissions,[1] chemical manufacturing represents a major contributor to global warming. However, with the plummeting prices of renewable electricity and initiatives like the United States Department of Energy's (DOE) SunShot, which targets utility-scale photovoltaics electricity prices as low as 3 ¢/kWh by 2030,[2] decarbonizing chemical manufacturing through electrification is becoming a feasible contributor towards net zero emissions. One promising technology for chemical industry decarbonization is the electrochemical carbon dioxide reduction reaction ($CO_2RR$), which has shown significant potential in converting captured $CO_2$ into value-added fuels and chemicals while utilizing intermittent renewable energy sources such as solar or wind.[3,4]

Among different $CO_2RR$ products, liquid fuels and chemicals are particularly intriguing given their high energy densities, as well as their versatile storage and distribution.[5] While several liquid products have been demonstrated with reasonable energy efficiencies using different electrocatalysts, formate/formic acid ($HCOO^-$/HCOOH) is the most promising for short-term commercialization opportunities. Formic acid has been used in various industries, including pharmaceuticals and biofuel manufacturing,[6,7] besides its potential to serve as a hydrogen carrier.[8] Furthermore, industrially relevant $CO_2RR$ performances have been reported for this reaction, with partial current densities reaching as high as 2.5 A $cm^{-2}$ and more than 80% Faradaic efficiency.[9] A cornerstone that made this mature performance possible is the adoption of gas diffusion electrodes (GDEs), which paved the way for high-performance gas-fed $CO_2RR$ electrolyzers.[10−12] However, conventional $CO_2RR$ electrolyzers rely on liquid electrolytes to transport generated liquid molecules and conduct electricity, necessitating energy- and cost-intensive downstream separation processes to recover high-purity liquid products and electrolytes separately.[5,13] Additionally, the carbon losses through (bi)carbonate formation, a thermodynamically favorable reaction between reactant $CO_2$ and hydroxide ($OH^-$) ions that are present in either the electrolyte reservoir or that are generated at the GDE/membrane interface, limit the $CO_2$ single-pass conversion efficiency (SPCE) in these systems and negatively affect the overall process energetics.[14−18] Some of the previous studies targeting high $CO_2$ SPCE restricted the input $CO_2$ to levels that compromised the electrolyzer performance, resulting in lower

**Received:** October 8, 2024
**Revised:** December 17, 2024
**Accepted:** December 20, 2024






https://doi.org/10.1021/acsenergylett.4c02773
*ACS Energy Lett.* 2025, 10, 450−458

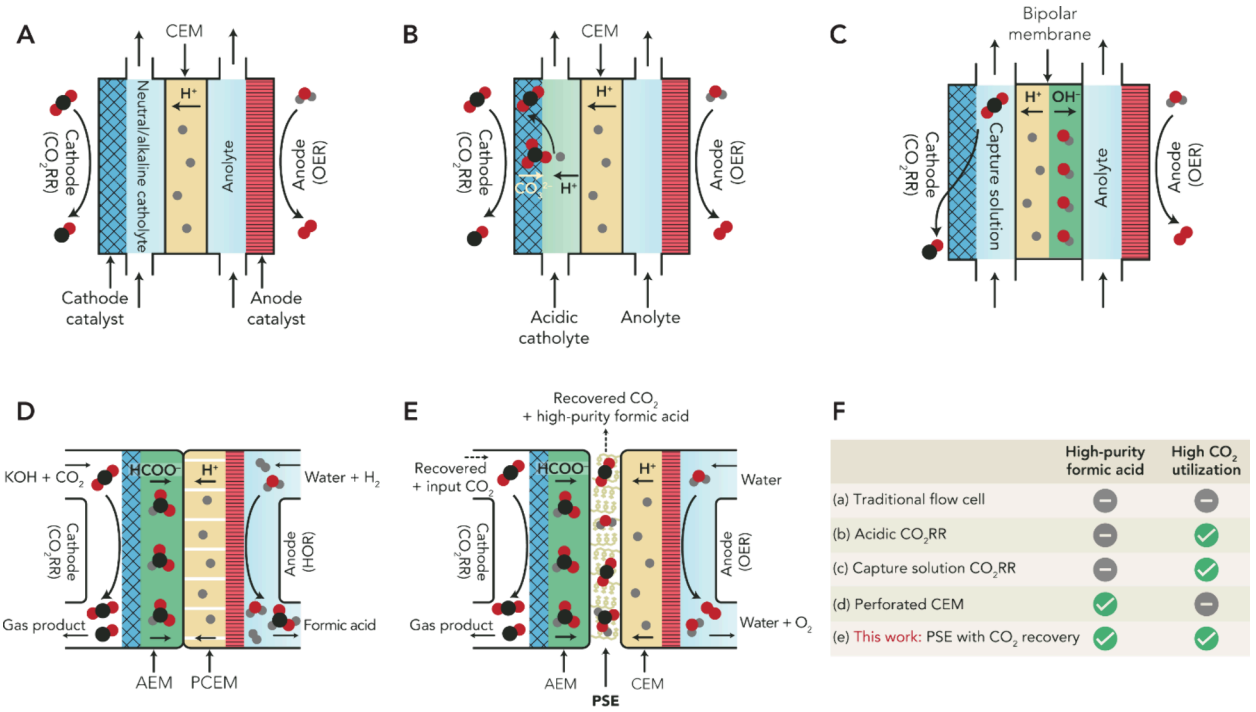


**Figure 1. Comparison of different $CO_2$RR electrolyzers for liquid product generation. (A) A schematic of the traditional flow cell reactor, which typically contains an alkaline or neutral catholyte for $CO_2$RR liquid product collection. This reactor produces formate salts mixed with impurity ions in the catholyte with low $CO_2$ utilization due to carbonate formation. (B) A schematic of acidic $CO_2$RR systems that employ an acidic catholyte to enable high $CO_2$ SPCE by regenerating carbonate ions as $CO_2$. These systems produce formic acid mixed with high-concentration supporting electrolytes. (C) A schematic of the capture solution $CO_2$RR systems, which may include (bi)carbonate electrolysis or amine-$CO_2$ adducts reduction. They achieve high $CO_2$ SPCE but are unable to produce electrolyte-free liquid products. (D) A schematic of the perforated-CEM electrolyzer, which comprises an AEM on the cathode side and a perforated CEM on the anode side. With hydrogen oxidation reaction (HOR) on the anode side, this setup produces high-purity formic acid in the anode stream, but carbonate formation still results in low $CO_2$ SPCE. (E) A schematic of the proposed PSE electrolyzer with $CO_2$ recovery. The PSE middle layer facilitates high-purity formic acid generation and offers an avenue to recover the lost $CO_2$, enabling high $CO_2$ SPCE. (F) A summary comparison of the systems presented here. PSE reactor with $CO_2$ recovery is the only system that can attain both high-purity formic acid generation and high $CO_2$ SPCE.**

target product Faradaic efficiency and higher cell voltage. This approach is impractical from an energy efficiency perspective, even when considering the potential benefits of downstream gas separation.[19−21]

Herein, we aim to hit two targets with one arrow by designing a $CO_2$RR system that efficiently produces high-purity formic acid while also operating at high $CO_2$ SPCE without compromising key performance metrics such as cell voltage and Faradaic efficiencies (FEs). Figure 1 displays different types of gas-fed $CO_2$RR reactor configurations reported in previous studies. We evaluated their potential to attain the two targets outlined here: high-purity formic acid production and high $CO_2$ utilization. Figure 1A depicts the traditional three-electrode flow cell configuration, in which a neutral/alkaline supporting catholyte is used, resulting in low $CO_2$ SPCE due to the reaction between gaseous $CO_2$ and the supporting electrolyte. Additionally, the product is formate salts mixed with the catholyte. Figure 1B shows acidic $CO_2$RR, which uses an acidic catholyte to achieve a higher $CO_2$ SPCE compared to alkaline or neutral $CO_2$RR. Yet, this configuration requires high-concentration supporting electrolytes to suppress the competing hydrogen evolution reaction (HER),[22−26] leading to a product mixture of formic acid and high-concentration supporting electrolytes. Another approach for high $CO_2$ SPCE is the direct $CO_2$RR of capture solutions[27] such as (bi)carbonates[28,29] or amine-$CO_2$ adducts,[30,31] as shown in Figure 1C. Nevertheless, the capture solution would be mixed with the liquid product in this scenario. More recently, Neyerlin et al.[32] reported an interesting perforated-CEM (PCEM) cell architecture to produce high-purity formic acid, as displayed in Figure 1D. However, this approach still does not limit carbon losses caused by the carbonate crossover to the anode side. Besides, high input $CO_2$ flow rates are required to sustain the biphasic flow on the backside of the cathode GDE. Another potential reactor design is the innovative microchanneled CEM design developed by Sinton et al.[33] While promising, the scalability limitations of soft lithography require careful consideration when implementing this design.

In this work, we propose using the three-chamber porous solid electrolyte (PSE) cell shown in Figure 1E to address these two challenges. The PSE reactor design has been reported and optimized for high-purity formic acid generation in previous studies,[34−37] and its capability to convert $CO_2$ to CO with high SPCE has been demonstrated.[15] Yet, the challenge of achieving high-purity liquid products under high $CO_2$ SPCE conditions remains elusive. The modular PSE design[38] is suitable for our aims here, as it introduces a porous ion-exchange resin layer between a CEM on the anode side and an AEM on the cathode side, adding a buffer region from which we can collect high-purity formic acid by flowing deionized water and recover $CO_2$ losses through a neutraliza-


https://doi.org/10.1021/acsenergylett.4c02773
ACS Energy Lett. 2025, 10, 450−458

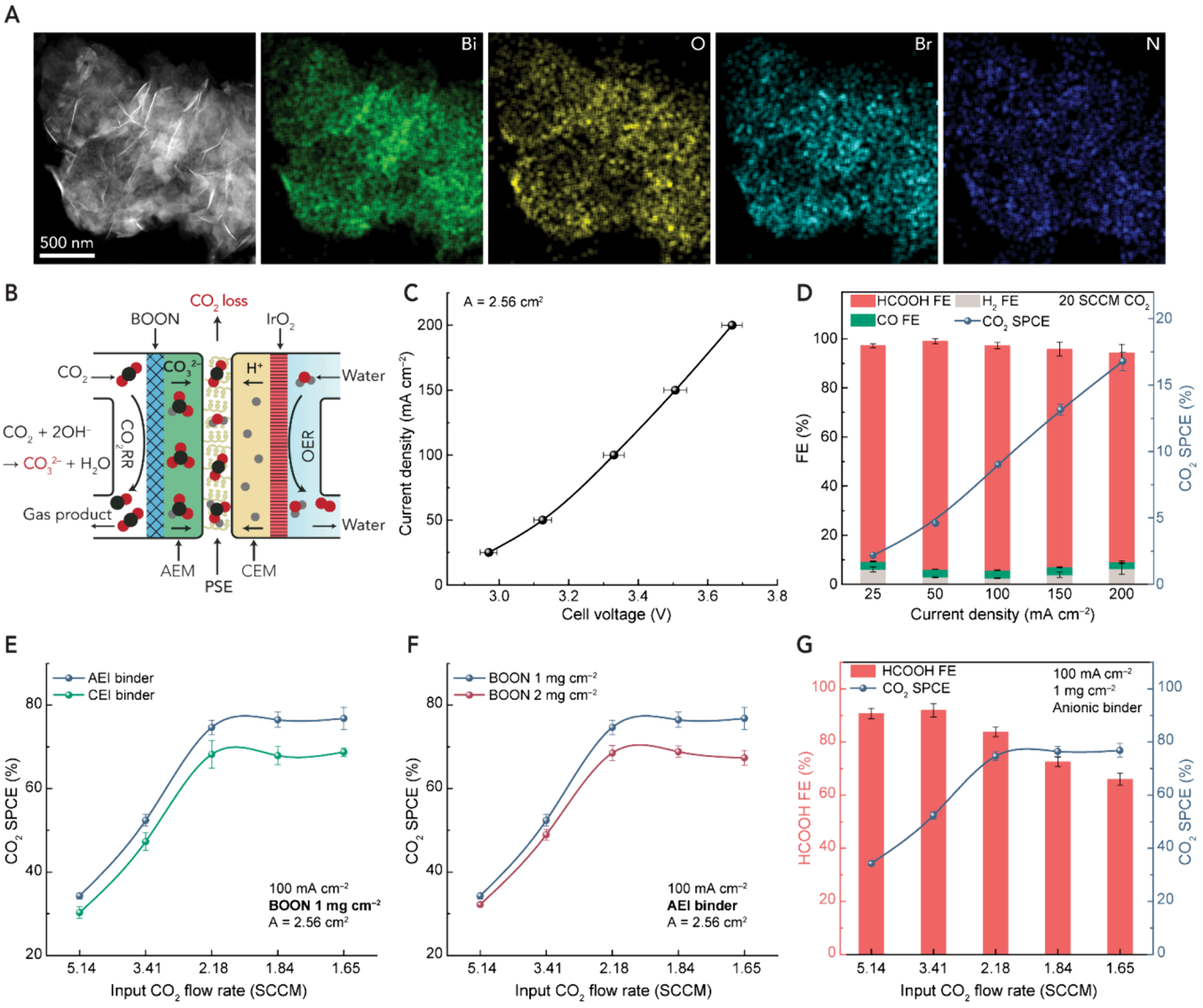


**Figure 2. Electrochemical performance of $CO_2$RR to HCOOH in the PSE reactor without $CO_2$ recovery. (A) A HAADF image of the synthesized BOON catalyst with the corresponding TEM-EDS mapping showing the uniformity of the elements introduced during the hydrolysis synthesis. (B) A schematic illustration of the PSE reactor consisting of a BOON cathode catalyst, a PiperION AEM, a middle layer of cation-exchange resins for high-purity HCOOH generation, a Nafion 117 CEM, and an $IrO_2$ anode. The illustration showcases the carbonate formation and carbon losses associated with the PSE system. (C) The *IV* curve of the BOON catalyst in the PSE reactor with a catalyst area of 2.56 $cm^2$ and a 20 SCCM $CO_2$ gas input. (D) The corresponding FE and $CO_2$ SPCE of the BOON catalyst under various current densities in the PSE reactor with a catalyst area of 2.56 $cm^2$ and a 20 SCCM $CO_2$ gas input. (E) The effect of the binder identity, comparing CEI vs AEI, on the $CO_2$ SPCE with a fixed catalyst loading of 1 mg $cm^{-2}$ in the PSE reactor at 100 mA $cm^{-2}$ while varying the input $CO_2$ flow rates. (F) The effect of the BOON catalyst loading (1 vs 2 mg $cm^{-2}$) on the $CO_2$ SPCE with an AEI binder in the PSE reactor at 100 mA $cm^{-2}$ while varying the input $CO_2$ flow rates. (G) The HCOOH FE and the corresponding $CO_2$ SPCE using the conditions optimized for SPCE (1 mg $cm^{-2}$ BOON catalyst loading with an AEI binder) at 100 mA $cm^{-2}$ with various input $CO_2$ flow rates in the PSE reactor without $CO_2$ recovery. Measurements were taken at least three times, and the average values are shown with the standard deviation as error bars.**

tion reaction between the (bi)carbonate ions from the cathode side and protons from the anode side. The regenerated $CO_2$ gas from the PSE layer can be refed into the cathode chamber to improve the carbon utilization efficiency during $CO_2$RR. By implementing the PSE design, we successfully demonstrated a $CO_2$-to-HCOOH operation with a $CO_2$ SPCE of 95.1 ± 1.7% at 100 mA $cm^{-2}$. We then showcased a stable performance for 100 h at 100 mA $cm^{-2}$. Integrating this $CO_2$RR PSE reactor with our recently reported PSE carbon capture reactor,[39] we successfully designed a sequential carbon capture and conversion system that can efficiently and continuously convert simulated flue gas (10% $CO_2$, 10% $O_2$, and balance $N_2$) into a high-purity formic acid solution with high $CO_2$ SPCE.

We first sought to optimize the $CO_2$ SPCE in the PSE reactor without $CO_2$ recovery. The middle layer of the PSE consisted of ion-exchange resin particles made of styrene-divinylbenzene with sulfonic acid functional groups and an average diameter of 200 $\mu$m (Figure S1), enabling high-purity formic acid generation that was collected by a deionized water stream. On the cathode side, we used a scalable, well-established, formate-producing catalyst: layered basic bismuth


https://doi.org/10.1021/acsenergylett.4c02773
ACS Energy Lett. 2025, 10, 450−458

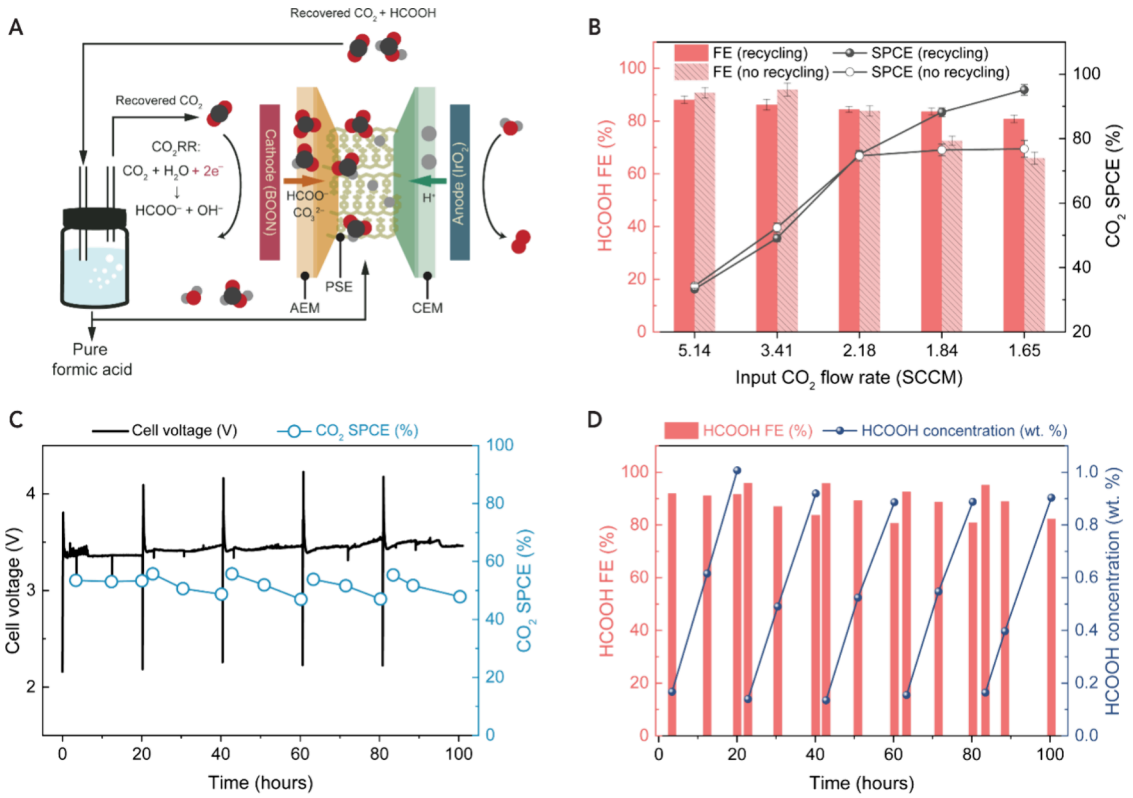


**Figure 3. Electrochemical performance of the PSE reactor with $CO_2$ recovery for high-purity HCOOH generation and high $CO_2$ SPCE using the BOON catalyst. (A) A schematic illustration of the PSE reactor with $CO_2$ recovery through recycling the $CO_2$ that crosses over to the middle layer back to the reactant stream. The PSE reactor uses a BOON cathode catalyst (A = 2.56 $cm^2$), a PiperION AEM, a cation-exchange resin in the middle layer, a Nafion 117 CEM, and an $IrO_2$ anode. (B) The HCOOH FE and $CO_2$ SPCE of the PSE reactor with and without $CO_2$ recycling at 100 mA $cm^{-2}$ with various input $CO_2$ flow rates. $CO_2$ recovery through recycling the middle layer $CO_2$ reaches a high $CO_2$ SPCE of 95.1 ± 1.7%, ~20% higher SPCE compared to the case of no recycling while maintaining more than 80% HCOOH FE. Measurements were taken at least three times, and the average values are shown with standard deviation as error bars. The PSE with $CO_2$ recovery 100-h stability at 100 mA $cm^{-2}$ with 3.34 SCCM of $CO_2$ input using the BOON catalyst with (C) the corresponding cell potential and $CO_2$ SPCE and (D) HCOOH FE and concentration in wt %. The stability test was carried out in 20-h cycles, and the voltage dips correspond to instances where the cell was stopped, and the product HCOOH was collected.**

nitrate $Bi_6O_6(OH)_3(NO_3)_3 \cdot 1.5H_2O$ (BOON; Figure 2A), which our group previously reported.[35] The anode side reaction was oxygen evolution reaction (OER) on an iridium oxide ($IrO_2$) catalyst. Besides unreacted $CO_2$, the carbon losses in this system were due to the carbonate formation reaction on the cathode side, after which the carbonate ions cross the AEM and into the middle layer, as shown in Figure 2B.

We aimed to evaluate the performance of $CO_2RR$ to formic acid and study its associated carbon losses in the PSE reactor. The synthesized BOON catalyst had a nanosheet morphology (Figure S2) with a uniform distribution of its constituent elements (Bi, O, Br, and N), as evidenced by the high-angle annular dark-field (HAADF) image and the transmission electron microscopy energy-dispersive X-ray spectroscopy (TEM-EDS) mapping in Figure 2A. Post-reaction BOON confirmed the removal of Br based on XPS and TEM results (Figures S3 and S4). The BOON catalyst proved to be highly active and selective toward HCOOH in the PSE reactor, with HCOOH as the sole liquid product detected using NMR (Figure S5). Besides, it delivered a current density of 200 mA $cm^{-2}$ with a cell voltage below 3.7 V while maintaining HCOOH FE above 85% (Figures 2C and 2D). Please note that all the two-electrode full-cell voltages reported in this study were not subjected to any *iR* compensation. Gas chromatography (GC; Figure S6) was used to quantify the gas products (CO and $H_2$) from the BOON PSE, which stayed below a total of 15% under the current densities explored here (25 to 200 mA $cm^{-2}$). At an input $CO_2$ flow rate of 20 SCCM, the maximum $CO_2$ SPCE was below 17%, observed at 200 mA $cm^{-2}$, as illustrated in Figure 2D. The details of the SPCE quantification method are included in the Experimental Procedures in the Supporting Information.

We then targeted higher $CO_2$ SPCE in this PSE system by first lowering the input $CO_2$ flow rate. Furthermore, we identified two other potential knobs to optimize the $CO_2$ SPCE: binder selection and catalyst loading. We reasoned that these two factors could help control the local reaction environment, which is key to enhancing the $CO_2$ SPCE, as the carbon loss phenomenon is highly dependent on the identity of the ions crossing the catalyst/membrane interface and their associated mass transfer. For binder selection, we chose a cation-exchange ionomer (CEI) and an anion-exchange ionomer (AEI) (Nafion and Sustainion). The CEI was selected for its fixed negative charge, which promotes the transport of positively charged ions, while the AEI, with its fixed positive charge, was selected to facilitate the transport of negatively charged ions. We compared the performance of both binders at a fixed catalyst loading of 1 mg $cm^{-2}$, a current density of 100 mA $cm^{-2}$ (total current of 256 mA; theoretical $CO_2$ consumption of 1.94 SCCM, assuming a 100% FE toward


https://doi.org/10.1021/acsenergylett.4c02773
ACS Energy Lett. 2025, 10, 450−458

a 2-electron transfer process), and input $CO_2$ gas flow rates ranging from 5.14 to 1.65 SCCM. We found that an AEI consistently outperformed the CEI in delivering superior $CO_2$ SPCE. Using an AEI, we achieved a maximum $CO_2$ SPCE of 76.8% at a $CO_2$ input of 1.65 SCCM (HCOOH FE of 65.9%) compared to 68.7% $CO_2$ SPCE (HCOOH FE of 59%) when using a CEI (Figure 2E). This enhanced $CO_2$ SPCE when using an anion-exchange binder can be attributed to the fact that Sustainion has been shown to help transport hydroxide ions away from the catalyst surface.[40] In contrast, Nafion increases the residence time of $OH^-$ ions at the catalyst/AEM interface, enhancing the probability of (bi)carbonate formation through the reaction between the input $CO_2$ gas and hydroxide ions, leading to more carbon losses. Using Sustainion binder, we then varied the catalyst loading from 1 to 2 mg $cm^{-2}$ to study the effect of a thicker catalyst layer on the $CO_2$ SPCE. As shown in Figure 2F, the higher BOON loading of 2 mg $cm^{-2}$ negatively affected the $CO_2$ SPCE compared to 1 mg $cm^{-2}$ with a $CO_2$ SPCE difference of more than 9% at 1.65 SCCM $CO_2$ input (76.8% for 1 mg $cm^{-2}$ vs 67.4% for 2 mg $cm^{-2}$). We hypothesize that the lower $CO_2$ SPCE is due to the fact that, under the same hydroxide ion flux, a thicker catalyst layer increases the reaction zone between gaseous $CO_2$ and $OH^-$ ions, leading to higher carbon losses. This can be corroborated by the recent model developed by Lees et al.,[16] where the authors observed a similar correlation between the catalyst layer thickness and carbon losses. With the optimal binder (AEI rather than CEI) and catalyst loading (1 mg $cm^{-2}$ as opposed to 2 mg $cm^{-2}$), the $CO_2$ SPCE was improved from 34.3% to 76.8%, as the $CO_2$ input was decreased from 5.14 to 1.65 SCCM (Figure 2G). Based on eqs 1 and 2, the theoretical $CO_2$ SPCE of the 2-electron reduction of $CO_2$ to formate should be capped at 67%.

$$CO_2(g) + H_2O(l) + 2e^- \rightarrow HCOO^- + OH^- \quad (1)$$

$$CO_2 + 2OH^- \rightarrow CO_3^{2-} + H_2O \quad (2)$$

This maximum $CO_2$ SPCE theoretical guideline presumes that all the $OH^-$ ions produced during the electrochemical $CO_2$RR in eq 1 react with gaseous $CO_2$, forming carbonate before crossing the AEM. However, if $OH^-$ ions are efficiently transported away from the catalyst layer, fewer $CO_2$ molecules will cross the AEM, and more $CO_2$ can participate directly in the $CO_2$RR reaction, pushing the SPCE beyond this theoretical limit. Our results showing a maximum of 76.8% $CO_2$ SPCE under optimized conditions were further supported by a carbon balance that indicated a measured ratio of around 3 for reacted/crossover $CO_2$ (see Figure S7). These findings suggest that the established theoretical guideline has limitations that could be overcome by optimizing the $CO_2$RR reaction environment through tuning key parameters such as binder choice and catalyst loading.

Even though the results discussed here showed that the $CO_2$ SPCE can be optimized up to 76.8%, the HCOOH FE started to decline as the input $CO_2$ flow rate was decreased below 3.41 SCCM, reaching a minimum of 65.9% at the lowest $CO_2$ gas input (Figure 2G). However, from an overall energy expenditure perspective, optimizing the $CO_2$ SPCE at the expense of FE is not always feasible.[19−21] Therefore, we sought to preserve the FE while reaching even higher $CO_2$ SPCE by taking advantage of the PSE design and recovering the lost $CO_2$.

As discussed earlier, the PSE reactor offers the advantage of producing high-purity formic acid while allowing for the possibility of leveraging ionic movements for $CO_2$ recovery. As represented in Figure 3A, the solid-electrolyte layer serves as a buffer zone, in which the (bi)carbonate ions traveling across the cathode/AEM interface are met with the protons coming from the anodic oxygen evolution reaction. This leads to a neutralization reaction that releases $CO_2$ gas, given that the input deionized water stream is saturated with $CO_2$. Using the optimized conditions from the previous section (Sustainion binder and 1 mg $cm^{-2}$ BOON loading), we tested the PSE configuration at 100 mA $cm^{-2}$ while refeeding the unreacted $CO_2$ from the middle layer back to the cathode side (Figure S8). As shown in Figure 3B, we found the HCOOH FE remained above 80%, as the input $CO_2$ gas flow rate was decreased from 5.14 to 1.65 SCCM. This indicates that recycling the $CO_2$ from the middle layer could allow for a high HCOOH FE even at reduced $CO_2$ gas inputs. When compared to the case of no $CO_2$ recycling at a $CO_2$ input of 1.65 SCCM, recovering the $CO_2$ losses using the PSE reactor shows a notable maximum $CO_2$ SPCE of 95.1 ± 1.7% (76.8 ± 2.6% for no recycling) with HCOOH FE of 80.8 ± 1.4% (65.9 ± 2.3% for no recycling). This represents an approximately 20% improvement in $CO_2$ SPCE when recovering the $CO_2$ losses compared to the control case of no recycling.

We then designed a stability experiment to examine the durability of this $CO_2$ recycling approach. To exclude other factors that could influence the device stability and provide a fair investigation regarding the stability of the PSE $CO_2$ recovery system, we chose to keep the formic acid concentration inside the middle layer below 1 wt % by collecting the product formic acid after every 20-h cycle and flushing the middle layer with DI water to remove any residual formic acid before initiating the following cycle (Voltage dips; Figure 3C). We also set the input $CO_2$ gas to 3.34 SCCM and operated under a current density of 100 mA $cm^{-2}$ (total current of 256 mA) throughout the stability test. As shown in Figures 3C and 3D, the system showed excellent stability over 100 h (five 20-h cycles), consistently maintaining an HCOOH FE of 80−95% and a $CO_2$ SPCE 47−55%. Each cycle produced 400 mL of ∼1 wt % high-purity formic acid. SEM images of the post-stability BOON catalyst (Figure S9) show that the catalyst morphology transformed from the initial nanosheet structure to nanoparticles while still preserving its activity and selectivity toward HCOOH, as evidenced by the stability test. Further reducing the $CO_2$ input from 3.34 SCCM to 1.9 SCCM while testing the durability at 100 mA $cm^{-2}$ still yielded encouraging results of HCOOH FE and $CO_2$ SPCE above 90% at the start of all five cycles, as shown in Figure S10. However, the performance decreased to a low HCOOH FE between 62 and 76% FE at the end of each cycle. The performance decline can be attributed to HCOOH back diffusion, which becomes more pronounced as its concentration increases during each cycle. Alternatively, this could be linked to GDL flooding, which might have a more significant impact on performance under low $CO_2$ inputs. These open questions should be reconciled in future studies.

In addition to enhancing the $CO_2$ SPCE and producing high-purity formic acid, we wanted to take a step further toward the practical deployment of the $CO_2$RR technology by investigating the feasibility of flue gas conversion to formic acid. However, flue gas conversion to value-added products using $CO_2$RR encounters challenges such as the presence of


https://doi.org/10.1021/acsenergylett.4c02773
ACS Energy Lett. 2025, 10, 450−458

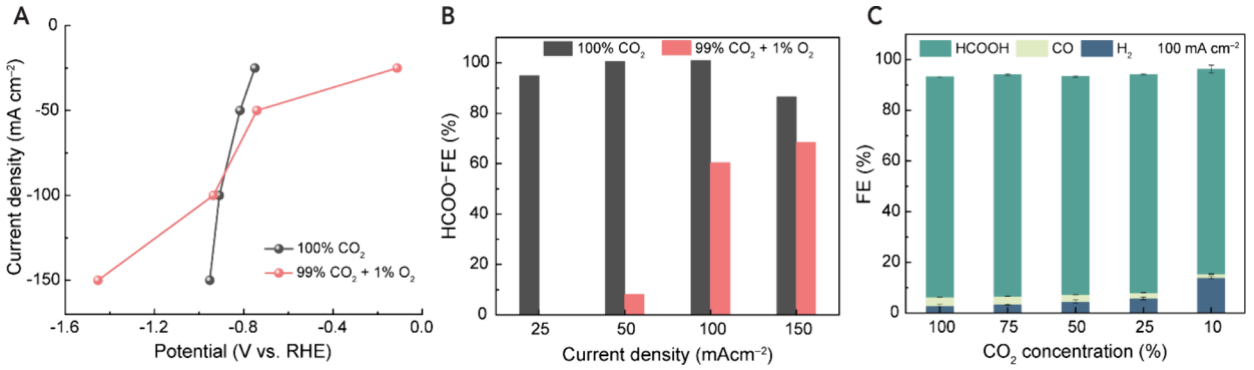


**Figure 4. The effect of oxygen presence and low $CO_2$ concentrations on the electrochemical $CO_2$ RR performance. The effect of $O_2$ presence on the $CO_2$RR performance in a standard three-electrode flow cell. The introduction of 1% $O_2$ shifted the performance to ORR instead of $CO_2$RR, especially at low current densities, evidenced by (A) The *IV* curve with 80% *iR* compensation and (B) the formate FE. The gas input was fixed at 100 SCCM. The three-electrode flow cell consisted of a BOON catalyst as the working electrode, 1 M $KHCO_3$ catholyte, an SCE reference electrode, Nafion 117 CEM, 1 M KOH anolyte, and a Ni foam anode with an active area of 1 $cm^2$. (C) FE of HCOOH, $H_2$, and CO as a function of the input $CO_2$ concentration when using an input mixture of $CO_2$ and Ar at a total of 100 SCCM in the PSE reactor without $CO_2$ recovery at 100 mA $cm^{-2}$ and a BOON catalyst area of 2.56 $cm^2$.**

impurities (e.g., $SO_x$, $NO_x$), high temperatures and pressures, oxygen presence, and low $CO_2$ concentrations. We chose to focus on two prominent challenges—oxygen presence and low $CO_2$ concentrations—and developed a series of experiments to isolate and evaluate the impact of each factor on the $CO_2$RR performance. We used a standard three-electrode flow cell to investigate the intrinsic effects of introducing oxygen on the BOON performance. We started by benchmarking performance in the flow cell using a 1 $cm^2$ active area with a total $CO_2$ input of 100 SCCM while increasing the current density from 25 to 150 mA $cm^{-2}$ and found that the BOON catalyst could deliver up to 150 mA $cm^{-2}$ at −0.95 V vs RHE with ∼86% FE toward $HCOO^-$. We then introduced 1% $O_2$ while keeping the total input flow rate at 100 SCCM (99 SCCM $CO_2$ + 1 SCCM $O_2$) and noticed drastic differences in the half-cell potential and the $CO_2$RR FE. As the *IV* curve in Figure 4A shows, the half-cell potential for 1% $O_2$ was −0.11 V vs RHE under −25 mA $cm^{-2}$; this is 0.64 V lower than the 100% $CO_2$ case at the same current density, which could be explained by the fact the current was exclusively used toward oxygen reduction reaction (ORR)[41] with no $CO_2$RR observed. This was confirmed by the NMR results in Figure 4B, where no formate product was detected at 25 mA $cm^{-2}$. As the current density was ramped up to 50, 100, and 150 mA $cm^{-2}$, the $HCOO^-$ FE gradually increased to 8%, 60%, and 68%, respectively. Although more formate was collected at higher currents for 1% $O_2$, the $HCOO^-$ FEs were significantly lower than the control case of 100% $CO_2$. These results confirm that introducing even as little as 1% $O_2$ would significantly worsen the $CO_2$RR performance.

We then aimed to isolate the effect of low $CO_2$ concentration on the $CO_2$RR-to-HCOOH reaction. To stay consistent with the system presented earlier, we tested the $CO_2$ concentration effects in a PSE electrolyzer to produce high-purity formic acid while fixing the applied current density at 100 mA $cm^{-2}$ and varying the input gas $CO_2$ concentrations starting from 100% and going down to 10% by introducing a mixture of $CO_2$ and argon. As shown in Figure 4C, decreasing the $CO_2$ concentration from 100% to 10% at 100 mA $cm^{-2}$ resulted in an increased HER from ∼3% to ∼14% and an associated decrease in $CO_2$RR. Although the effect of lower $CO_2$ concentration on the $CO_2$RR performance is not as detrimental as $O_2$ presence, operating at $CO_2$ concentrations of 10% or lower—levels typical of flue gas sources[4,42]—will likely result in compromised $CO_2$RR performance. Therefore, to attain successful flue gas conversion to $CO_2$RR products, it is essential to develop a system capable of continuously capturing highly concentrated $CO_2$ while remaining tolerant to the oxygen present in flue gas sources.

Hence, there is a need to introduce a carbon capture step that captures and regenerates high-purity $CO_2$ gas that can be fed to the $CO_2$RR electrolyzer. However, typical carbon capture systems operate in batches, relying on sorbent charge and discharge processes to capture and release $CO_2$,[43,44] which constrains the implementation of a continuous sequential system of $CO_2$ capture followed by $CO_2$ reduction. To address this, we introduce a sequential system, where simulated flue gas is first fed to a $CO_2$ capture PSE electrolyzer that continuously releases pure $CO_2$ gas from the middle layer, which is then fed to a $CO_2$ reduction PSE electrolyzer that produces high-purity formic acid while recovering $CO_2$ losses to achieve a high $CO_2$ SPCE. As depicted in Figure 5A, the $CO_2$ capture device is a PSE architecture that we recently reported,[39] where simulated flue gas (10% $CO_2$, 10% $O_2$, balance $N_2$) is fed to the cathode side. The *IV* curve of the $CO_2$ capture device is shown in Figure S11. In this device, we fully utilize the oxygen present in point sources by performing ORR on a platinum-on-carbon (Pt/C) cathode that generates hydroxide ions, creating a highly alkaline environment that efficiently and continuously absorbs $CO_2$ as carbonate ions. These ions then migrate across the AEM and into the middle layer, where they react with protons generated by the anodic OER. This reaction enables the release of high-purity $CO_2$ gas from the middle layer, provided that the middle layer solution is saturated with $CO_2$, which can be achieved by recycling the deionized water in the middle layer until saturation. Figure 5B shows the successful implementation of this proposed capture−reduction sequential system for flue gas conversion to formic acid. We operated the ORR/OER cell at 50 mA $cm^{-2}$ (312.5 mA total current), with the captured $CO_2$ gas fed to the $CO_2$RR cell, which was operated at 100 mA $cm^{-2}$ (256 mA total current). Similar to the test in Figure 3, we limited the formic acid concentration to below 1 wt % by controlling the recycled middle layer volume in the $CO_2$RR cell and refreshing the middle layer


https://doi.org/10.1021/acsenergylett.4c02773
ACS Energy Lett. 2025, 10, 450−458

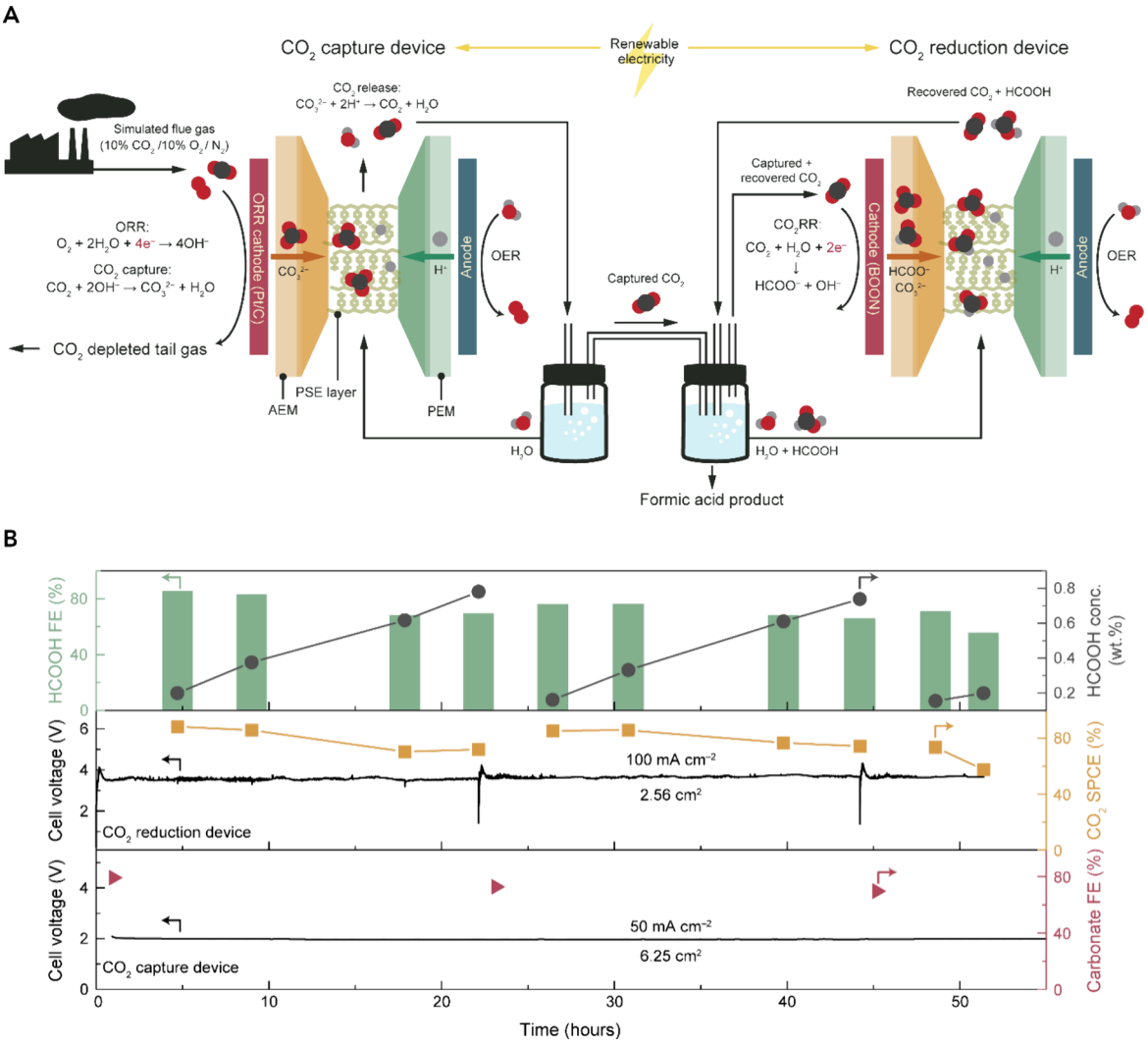


**Figure 5. A demonstration of the continuous $CO_2$ capture−$CO_2$ reduction sequential system for simulated flue gas conversion to high-purity formic acid with high $CO_2$ utilization. (A) A schematic illustration of the continuous $CO_2$ capture−$CO_2$RR sequential system. Simulated flue gas (10% $CO_2$, 10% $O_2$, balance $N_2$) was fed to a $CO_2$ capture PSE reactor, in which $CO_2$ was captured via electrochemical ORR and released as pure $CO_2$ gas, which was then fed to a $CO_2$RR PSE to produce high-purity formic acid with high $CO_2$ SPCE through recovering the lost $CO_2$. (B) Experimental demonstration of the continuous simulated flue gas (10% $CO_2$, 10% $O_2$, balance $N_2$) conversion to high-purity formic acid in the sequential $CO_2$ capture−$CO_2$RR. The ORR/OER PSE $CO_2$ capture cell was operated at 50 mA $cm^{-2}$ with an active area of 6.25 $cm^2$ using Pt/C as an ORR catalyst and $IrO_2$ as an OER catalyst. The $CO_2$RR PSE cell was operated at 100 mA $cm^{-2}$ using 2.56 $cm^2$ BOON as a $CO_2$RR catalyst and $IrO_2$ as an OER catalyst.**

solution after around 20 h. The carbonate FE of the $CO_2$ capture system prior to the first $CO_2$RR cycle was measured at 79.2%, corresponding to an input $CO_2$ flow of 1.88 SCCM to the $CO_2$RR cell. The initial $CO_2$ SPCE was 88.4% at the start of the test, but it decreased to 71.9% by the end of the first cycle. This decrease resulted from a decline in the carbon capture efficiency, as evidenced by the drop in the carbonate FE after the first cycle, decreasing from 79.2% to 72.8% with a corresponding decrease in the $CO_2$ input from 1.88 SCCM in the first cycle to 1.72 SCCM. Even with 1.72 SCCM $CO_2$ input in the second cycle, the $CO_2$RR PSE delivered a high $CO_2$ SPCE of 85.6% at the beginning of the cycle, which then dropped to 74.3%. The declining $CO_2$ capture performance reached a 69.7% carbonate FE before the third cycle, translating to a $CO_2$ input of 1.65 SCCM to the $CO_2$RR reactor. At this low $CO_2$ input flow rate, the HCOOH FE dropped significantly, reaching 55.7%, making the $CO_2$ capture cell the limiting factor in this demonstration. In conclusion, the $CO_2$RR-to-HCOOH PSE with $CO_2$ recovery could operate stably as long as there is enough $CO_2$ input, which was proven by the stability test in Figure 3. The demonstration in Figure 5 confirms that the concept of the sequential $CO_2$ capture−$CO_2$ reduction system presented here is viable for the conversion of flue gas to value-added products. Notably, this sequential process can operate continuously, eliminating the need for regeneration steps typically required in conventional carbon capture systems.

In this work, we showcased the ability of the PSE platform to produce high-purity formic acid while reaching a high $CO_2$ SPCE of 95.1 ± 1.7% at 100 mA $cm^{-2}$ without sacrificing key performance metrics such as cell voltage or HCOOH FE. This high SPCE was achieved by systematically optimizing key parameters in the $CO_2$RR reaction environment, including the ionomer binder and catalyst loading, and by employing these optimal conditions in conjunction with recovering carbon losses from the PSE middle layer. We expanded the scope of


https://doi.org/10.1021/acsenergylett.4c02773
ACS Energy Lett. 2025, 10, 450−458

this work by exploring the feasibility of directly feeding simulated flue gas (10% $CO_2$, 10% $O_2$, balance Ar) into a $CO_2$RR cell and assessing the impacts of oxygen presence and low $CO_2$ concentrations. Finally, a $CO_2$ capture−$CO_2$ reduction sequential system was introduced to allow for continuous and efficient flue gas conversion to high-purity formic acid with high $CO_2$ SPCE. While the PSE design enables the application demonstrated in this study, incorporating an extra layer within the electrochemical reactor introduces ohmic losses, thereby reducing the overall energy efficiency. Future PSE designs should aim to reduce the middle layer thickness, potentially by incorporating resin wafers developed in the field of electrodeionization,[45] while also focusing on creating more ionically conductive PSE layers.

## ■ ASSOCIATED CONTENT

### Supporting Information

The Supporting Information is available free of charge at https://pubs.acs.org/doi/10.1021/acsenergylett.4c02773.

Experimental details, including PSE assembly and testing protocols, with additional Figures S1−S11 (PDF)

## ■ AUTHOR INFORMATION


### Corresponding Author

**Haotian Wang** − *Department of Chemical and Biomolecular Engineering, Rice University, Houston, Texas 77005, United States; Department of Materials Science and Nano Engineering, Department of Chemistry, and Rice Advanced Materials Institute, Rice University, Houston, Texas 77005, United States;* orcid.org/0000-0002-3552-8978; Email: htwang@rice.edu

### Authors

**Ahmad Elgazzar** − *Department of Chemical and Biomolecular Engineering, Rice University, Houston, Texas 77005, United States;* orcid.org/0000-0003-1453-4938

**Peng Zhu** − *Department of Chemical and Biomolecular Engineering, Rice University, Houston, Texas 77005, United States;* orcid.org/0000-0002-8855-0335

**Feng-Yang Chen** − *Department of Chemical and Biomolecular Engineering, Rice University, Houston, Texas 77005, United States;* orcid.org/0000-0002-3113-383X

**Shaoyun Hao** − *Department of Chemical and Biomolecular Engineering, Rice University, Houston, Texas 77005, United States;* orcid.org/0000-0001-8353-518X

**Tae-Ung Wi** − *Department of Chemical and Biomolecular Engineering, Rice University, Houston, Texas 77005, United States;* orcid.org/0000-0002-8295-825X

**Chang Qiu** − *Department of Chemical and Biomolecular Engineering, Rice University, Houston, Texas 77005, United States;* orcid.org/0000-0001-5462-7157

**Valery Okatenko** − *Department of Chemical and Biomolecular Engineering, Rice University, Houston, Texas 77005, United States;* orcid.org/0000-0002-7542-7995

Complete contact information is available at: https://pubs.acs.org/10.1021/acsenergylett.4c02773


### Author Contributions

Conceptualization, H.W. and A.E.; Experiments, A.E. and P.Z.; Characterization, A.E., F.-Y.C., S.H., T.-U.W., C.Q., and V.O.; Writing − original draft, A.E.; Writing − review and editing, A.E., H.W.; Funding and supervision, H.W.

### Notes

The authors declare no competing financial interest.

## ■ ACKNOWLEDGMENTS

This work was supported by the U.S. Department of Energy (Award Number: DE-EE0009287), the National Science Foundation (NSF EFRI Award Number: 2029442), the Robert A. Welch Foundation (Grant Number: C-2051-20230405), and the David and Lucile Packard Foundation (Grant Number: 2020-71371). The research was done in part using resources of the Shared Equipment Authority at Rice University (https://research.rice.edu/sea/). A.E. acknowledges the support from the Rice Chevron energy graduate fellowship from the Rice Sustainability Institute and Chevron.

## ■ REFERENCES


(1) Chemicals. IEA. https://www.iea.org/energy-system/industry/chemicals (accessed July 6, 2024).

(2) SunShot 2030. U.S. Department of Energy. https://www.energy.gov/eere/solar/sunshot-2030 (accessed July 6, 2024).

(3) De Luna, P.; Hahn, C.; Higgins, D.; Jaffer, S. A.; Jaramillo, T. F.; Sargent, E. H. What Would It Take for Renewably Powered Electrosynthesis to Displace Petrochemical Processes? *Science* **2019**, *364* (6438), No. eaav3506.

(4) O'Brien, C. P.; Miao, R. K.; Shayesteh Zeraati, A.; Lee, G.; Sargent, E. H.; Sinton, D. CO2 Electrolyzers. *Chem. Rev.* **2024**, *124* (7), 3648−3693.

(5) Zhu, P.; Wang, H. High-Purity and High-Concentration Liquid Fuels through CO2 Electroreduction. *Nat. Catal* **2021**, *4* (11), 943−951.

(6) Valentini, F.; Kozell, V.; Petrucci, C.; Marrocchi, A.; Gu, Y.; Gelman, D.; Vaccaro, L. Formic Acid, a Biomass-Derived Source of Energy and Hydrogen for Biomass Upgrading. *Energy Environ. Sci.* **2019**, *12* (9), 2646−2664.

(7) Nankya, R.; Elgazzar, A.; Zhu, P.; Chen, F.-Y.; Wang, H. Catalyst Design and Reactor Engineering for Electrochemical CO2 Reduction to Formate and Formic Acid. *Mater. Today* **2024**, *76*, 94.

(8) Crandall, B. S.; Brix, T.; Weber, R. S.; Jiao, F. Techno-Economic Assessment of Green H2 Carrier Supply Chains. *Energy Fuels* **2023**, *37* (2), 1441−1450.

(9) Peng, C.; Yang, S.; Luo, G.; Yan, S.; Chen, N.; Zhang, J.; Chen, Y.; Wang, X.; Wang, Z.; Wei, W.; Sham, T.-K.; Zheng, G. Ampere-Level CO2-to-Formate Electrosynthesis Using Highly Exposed Bismuth(110) Facets Modified with Sulfur-Anchored Sodium Cations. *Chem.* **2023**, *9* (10), 2830−2840.

(10) Higgins, D.; Hahn, C.; Xiang, C.; Jaramillo, T. F.; Weber, A. Z. Gas-Diffusion Electrodes for Carbon Dioxide Reduction: A New Paradigm. *ACS Energy Lett.* **2019**, *4* (1), 317−324.

(11) Lees, E. W.; Mowbray, B. A. W.; Parlane, F. G. L.; Berlinguette, C. P. Gas Diffusion Electrodes and Membranes for CO2 Reduction Electrolysers. *Nat. Rev. Mater.* **2022**, *7* (1), 55−64.

(12) Wakerley, D.; Lamaison, S.; Wicks, J.; Clemens, A.; Feaster, J.; Corral, D.; Jaffer, S. A.; Sarkar, A.; Fontecave, M.; Duoss, E. B.; Baker, S.; Sargent, E. H.; Jaramillo, T. F.; Hahn, C. Gas Diffusion Electrodes, Reactor Designs and Key Metrics of Low-Temperature CO2 Electrolysers. *Nat. Energy* **2022**, *7* (2), 130−143.

(13) Ramdin, M.; Morrison, A. R. T.; de Groen, M.; van Haperen, R.; de Kler, R.; Irtem, E.; Laitinen, A. T.; van den Broeke, L. J. P.; Breugelmans, T.; Trusler, J. P. M.; Jong, W. de; Vlugt, T. J. H. High-Pressure Electrochemical Reduction of CO2 to Formic Acid/Formate: Effect of pH on the Downstream Separation Process and Economics. *Ind. Eng. Chem. Res.* **2019**, *58* (51), 22718−22740.

(14) Rabinowitz, J. A.; Kanan, M. W. The Future of Low-Temperature Carbon Dioxide Electrolysis Depends on Solving One Basic Problem. *Nat. Commun.* **2020**, *11* (1), 5231.

(15) Kim, J. Y. T.; Zhu, P.; Chen, F.-Y.; Wu, Z.-Y.; Cullen, D. A.; Wang, H. Recovering Carbon Losses in CO2 Electrolysis Using a Solid Electrolyte Reactor. *Nat. Catal* **2022**, *5* (4), 288−299.
(16) Lees, E. W.; Bui, J. C.; Romiluyi, O.; Bell, A. T.; Weber, A. Z. Exploring CO2 Reduction and Crossover in Membrane Electrode Assemblies. *Nat. Chem. Eng.* **2024**, *1* (5), 340−353.
(17) Weng, L.-C.; Bell, A. T.; Weber, A. Z. Towards Membrane-Electrode Assembly Systems for CO2 Reduction: A Modeling Study. *Energy Environ. Sci.* **2019**, *12* (6), 1950−1968.
(18) Ma, M.; Clark, E. L.; Therkildsen, K. T.; Dalsgaard, S.; Chorkendorff, I.; Seger, B. Insights into the Carbon Balance for CO2 Electroreduction on Cu Using Gas Diffusion Electrode Reactor Designs. *Energy Environ. Sci.* **2020**, *13* (3), 977−985.
(19) da Cunha, S. C.; Resasco, J. Maximizing Single-Pass Conversion Does Not Result in Practical Readiness for CO2 Reduction Electrolyzers. *Nat. Commun.* **2023**, *14* (1), 5513.
(20) da Cunha, S. C.; Resasco, J. Insights from Techno-Economic Analysis Can. Guide the Design of Low-Temperature CO2 Electrolyzers toward Industrial Scaleup. *ACS Energy Lett.* **2024**, *9* (11), 5550−5561.
(21) Moore, T.; Oyarzun, D. I.; Li, W.; Lin, T. Y.; Goldman, M.; Wong, A. A.; Jaffer, S. A.; Sarkar, A.; Baker, S. E.; Duoss, E. B.; Hahn, C. Electrolyzer Energy Dominates Separation Costs in State-of-the-Art CO2 Electrolyzers: Implications for Single-Pass CO2 Utilization. *Joule* **2023**, *7* (4), 782−796.
(22) Huang, J. E.; Li, F.; Ozden, A.; Sedighian Rasouli, A.; García de Arquer, F. P.; Liu, S.; Zhang, S.; Luo, M.; Wang, X.; Lum, Y.; Xu, Y.; Bertens, K.; Miao, R. K.; Dinh, C.-T.; Sinton, D.; Sargent, E. H. CO2 Electrolysis to Multicarbon Products in Strong Acid. *Science* **2021**, *372* (6546), 1074−1078.
(23) Monteiro, M. C. O.; Dattila, F.; Hagedoorn, B.; García-Muelas, R.; López, N.; Koper, M. T. M. Absence of CO2 Electroreduction on Copper, Gold and Silver Electrodes without Metal Cations in Solution. *Nat. Catal* **2021**, *4* (8), 654−662.
(24) Gu, J.; Liu, S.; Ni, W.; Ren, W.; Haussener, S.; Hu, X. Modulating Electric Field Distribution by Alkali Cations for CO2 Electroreduction in Strongly Acidic Medium. *Nat. Catal* **2022**, *5* (4), 268−276.
(25) Qiao, Y.; Lai, W.; Huang, K.; Yu, T.; Wang, Q.; Gao, L.; Yang, Z.; Ma, Z.; Sun, T.; Liu, M.; Lian, C.; Huang, H. Engineering the Local Microenvironment over Bi Nanosheets for Highly Selective Electrocatalytic Conversion of CO2 to HCOOH in Strong Acid. *ACS Catal.* **2022**, *12* (4), 2357−2364.
(26) Shen, H.; Jin, H.; Li, H.; Wang, H.; Duan, J.; Jiao, Y.; Qiao, S.-Z. Acidic CO2-to-HCOOH Electrolysis with Industrial-Level Current on Phase Engineered Tin Sulfide. *Nat. Commun.* **2023**, *14* (1), 2843.
(27) Ozden, A.; García de Arquer, F. P.; Huang, J. E.; Wicks, J.; Sisler, J.; Miao, R. K.; O'Brien, C. P.; Lee, G.; Wang, X.; Ip, A. H.; Sargent, E. H.; Sinton, D. Carbon-Efficient Carbon Dioxide Electrolysers. *Nat. Sustain* **2022**, *5* (7), 563−573.
(28) Li, T.; Lees, E. W.; Zhang, Z.; Berlinguette, C. P. Conversion of Bicarbonate to Formate in an Electrochemical Flow Reactor. *ACS Energy Lett.* **2020**, *5* (8), 2624−2630.
(29) Gutiérrez-Sánchez, O.; de Mot, B.; Bulut, M.; Pant, D.; Breugelmans, T. Engineering Aspects for the Design of a Bicarbonate Zero-Gap Flow Electrolyzer for the Conversion of CO2 to Formate. *ACS Appl. Mater. Interfaces* **2022**, *14* (27), 30760−30771.
(30) Leverick, G.; Bernhardt, E. M.; Ismail, A. I.; Law, J. H.; Arifutzzaman, A.; Aroua, M. K.; Gallant, B. M. Uncovering the Active Species in Amine-Mediated CO2 Reduction to CO on Ag. *ACS Catal.* **2023**, *13* (18), 12322−12337.
(31) Lee, G.; Li, Y. C.; Kim, J.-Y.; Peng, T.; Nam, D.-H.; Sedighian Rasouli, A.; Li, F.; Luo, M.; Ip, A. H.; Joo, Y.-C.; Sargent, E. H. Electrochemical Upgrade of CO2 from Amine Capture Solution. *Nat. Energy* **2021**, *6* (1), 46−53.
(32) Hu, L.; Wrubel, J. A.; Baez-Cotto, C. M.; Intia, F.; Park, J. H.; Kropf, A. J.; Kariuki, N.; Huang, Z.; Farghaly, A.; Amichi, L.; Saha, P.; Tao, L.; Cullen, D. A.; Myers, D. J.; Ferrandon, M. S.; Neyerlin, K. C. A Scalable Membrane Electrode Assembly Architecture for Efficient Electrochemical Conversion of CO2 to Formic Acid. *Nat. Commun.* **2023**, *14* (1), 7605.
(33) Xu, Y.; Miao, R. K.; Edwards, J. P.; Liu, S.; O'Brien, C. P.; Gabardo, C. M.; Fan, M.; Huang, J. E.; Robb, A.; Sargent, E. H.; Sinton, D. A Microchanneled Solid Electrolyte for Carbon-Efficient CO2 Electrolysis. *Joule* **2022**, *6* (6), 1333−1343.
(34) Yang, H.; Kaczur, J. J.; Sajjad, S. D.; Masel, R. I. Electrochemical Conversion of CO2 to Formic Acid Utilizing Sustainion™ Membranes. *Journal of CO2 Utilization* **2017**, *20*, 208−217.
(35) Xia, C.; Zhu, P.; Jiang, Q.; Pan, Y.; Liang, W.; Stavitski, E.; Alshareef, H. N.; Wang, H. Continuous Production of Pure Liquid Fuel Solutions via Electrocatalytic CO2 Reduction Using Solid-Electrolyte Devices. *Nat. Energy* **2019**, *4* (9), 776−785.
(36) Fan, L.; Xia, C.; Zhu, P.; Lu, Y.; Wang, H. Electrochemical CO2 Reduction to High-Concentration Pure Formic Acid Solutions in an All-Solid-State Reactor. *Nat. Commun.* **2020**, *11* (1), 3633.
(37) Yang, H.; Kaczur, J. J.; Sajjad, S. D.; Masel, R. I. Performance and Long-Term Stability of CO2 Conversion to Formic Acid Using a Three-Compartment Electrolyzer Design. *Journal of CO2 Utilization* **2020**, *42*, 101349.
(38) Xia, C.; Xia, Y.; Zhu, P.; Fan, L.; Wang, H. Direct Electrosynthesis of Pure Aqueous H2O2 Solutions up to 20% by Weight Using a Solid Electrolyte. *Science* **2019**, *366* (6462), 226−231.
(39) Zhu, P.; Wu, Z.-Y.; Elgazzar, A.; Dong, C.; Wi, T.-U.; Chen, F.-Y.; Xia, Y.; Feng, Y.; Shakouri, M.; Kim, J. Y.; Fang, Z.; Hatton, T. A.; Wang, H. Continuous Carbon Capture in an Electrochemical Solid-Electrolyte Reactor. *Nature* **2023**, *618* (7967), 959−966.
(40) Nwabara, U. O.; Hernandez, A. D.; Henckel, D. A.; Chen, X.; Cofell, E. R.; de-Heer, M. P.; Verma, S.; Gewirth, A. A.; Kenis, P. J. A. Binder-Focused Approaches to Improve the Stability of Cathodes for CO2 Electroreduction. *ACS Appl. Energy Mater.* **2021**, *4* (5), 5175−5186.
(41) Xu, Y.; Edwards, J. P.; Zhong, J.; O'Brien, C. P.; Gabardo, C. M.; McCallum, C.; Li, J.; Dinh, C.-T.; Sargent, E. H.; Sinton, D. Oxygen-Tolerant Electroproduction of C2 Products from Simulated Flue Gas. *Energy Environ. Sci.* **2020**, *13* (2), 554−561.
(42) Uribe-Soto, W.; Portha, J.-F.; Commenge, J.-M.; Falk, L. A Review of Thermochemical Processes and Technologies to Use Steelworks Off-Gases. *Renewable and Sustainable Energy Reviews* **2017**, *74*, 809−823.
(43) Keith, D. W.; Holmes, G.; St. Angelo, D.; Heidel, K. A Process for Capturing CO2 from the Atmosphere. *Joule* **2018**, *2* (8), 1573−1594.
(44) Tan, W.-L.; Ahmad, A. L.; Leo, C. P.; Lam, S. S. A Critical Review to Bridge the Gaps between Carbon Capture, Storage and Use of CaCO3. *Journal of CO2 Utilization* **2020**, *42*, 101333.
(45) Lin, Y. J.; Henry, M. P.; Snyder, S. W. Electronically and Ionically Conductive Porous Material and Method for Manufacture of Resin Wafers Therefrom. US7452920B2, November 18, 2008. https://patents.google.com/patent/US7452920B2/en (accessed September 6, 2024).


https://doi.org/10.1021/acsenergylett.4c02773
*ACS Energy Lett.* 2025, 10, 450−458